Asociación Argentina
de Mecánica Computacional

Mecánica Computacional Vol XLII, pp. 1349-1358
A. Caggiano, G. Etse, P. Folino, M. Goldschmit, M. Pucheta, M. Storti (Eds.)
U. Berardi, D. Borelli, A. Caggiano, S. Flores Larsen, P. Folino (Issue eds.)
Buenos Aires, November 11-14, 2025

COMPUTATIONAL DESIGN OF BIOCOMPATIBLE MORTAR FOR ERICARIA AMENTACEA HABITAT RESTORATION: ENHANCING THE ECOLOGICAL VALUE OF COASTAL STRUCTURES

Lourdes Coronel[a,b], Mahdi Zanjani[a], Jacopo Cimini[c], Juan Hostos[d], Javier Mroginski[b], Valentina Asnaghi[c] and Antonio Caggiano[a,e]

[a]*University of Genova, Department of Civil, Chemical and Environmental Engineering. Genova, Italy, info@dicca.unige.it, https://dicca.unige.it/*

[b]*Universidad Nacional del Nordeste. Chaco, Argentina, https://www.ing.unne.edu.ar/*

[c]*University of Genova, Department of Earth, Environment and Life Sciences. Genova, Italy, distav@pec.unige.it, https://distav.unige.it/*

[d]*Universidad Nacional del Litoral, Centro de Investigación de Métodos Computacionales, Santa Fe, Argentina.*

[e]*LMNI, INTECIN, FIUBA, Universidad de Buenos Aires, Buenos Aires, Argentina.*

Keywords: *Ericaria amentacea*, ecological restoration, sustainable mortar, marine aggregates, computational design, shape and topology optimization.

Abstract. On the Ligurian coast (Italy), 3D-printed concrete units were deployed to promote the attachment and growth of *Ericaria amentacea*, a habitat-forming macroalga essential for biodiversity and carbon sequestration. Although these structures were succesfully colonized in both laboratory and field settings, their mechanical resistance proved insufficient under marine loading conditions, limiting their long-term applicability. In this context, the study developed alternative mortars using conventional fabrication methods, incorporating crushed seashells as a partial replacement for natural fine aggregate. The results show that shell-based mixtures maintain flexural strength while exhibiting lower air permeability and reduced capillary absorption coefficients—properties favorable for durability in marine environments. A computational design stage was also introduced to optimize the geometry of the units with respect to linear-elastic stiffness, while enforcing the biologically inspired surface inclination for algal settlement. This approach integrates biological and mechanical criteria and points toward more resilient designs under marine stresses, offering a scalable pathway for restoring *E. amentacea* habitats in the Mediterranean.

ISSN: 2591-3522 DOI: 10.70567/mc.v42.ocsid8325

1 INTRODUCTION

Forests of macroalgae belonging to the complex *Cystoseira* sensu lato, and particularly *Ericaria amentacea*, are key ecosystems in the Mediterranean. They act as habitat-forming species, maintain biodiversity, and contribute to the sequestration of blue carbon (Chemello et al., 2022). However, these populations have suffered a marked decline in recent decades due to pollution, coastal urbanization, and the intensification of extreme climatic events (Filbee-Dexter and Wernberg, 2018). On the Ligurian coast (Italy), the Vaia storm in 2018 caused severe damage and led to the construction of a concrete breakwater that removed natural habitats of *Ericaria amentacea*, further accelerating its local regression (Cavaleri et al., 2022). This situation reflects a broader regional challenge: the loss of structural marine habitats and the urgent need to develop effective restoration strategies.

Among the solutions tested in the Mediterranean, 3D-printed concrete units have shown the ability to promote the attachment and growth of *Ericaria amentacea*, confirming the biological feasibility of such interventions (Cimini, 2025). However, these structures proved to be mechanically fragile in marine environments, which limited their scalability and long-term application. This highlights the need to design cementitious materials that are both more resistant and more durable, while preserving ecological functionality and sustainability.

One promising approach is the incorporation of recycled marine aggregates. Previous studies have demonstrated that crushed seashells are chemically compatible with cementitious matrices and can be used as a partial replacement for natural fine aggregate, while also contributing to the valorization of an abundant waste material (Leite et al., 2024; Lata and Rocha, 2019). In this study, conventional mortar mixtures were developed with partial replacement of natural fine aggregate by crushed seashells.

In parallel with materials development, a computational design step is introduced so that unit shape is informed not only by biological criteria but also by mechanical performance. The adopted framework follows the shape/topology optimization methodology of Allaire et al. (2021) using an Eulerian level-set representation of geometry. The implementation is performed in `Gridap` (Julia), using the open-source `GridapTopOpt.jl` toolbox (Wegert et al., 2025) on a fixed Cartesian mesh. The optimization process was implemented to generate mechanically efficient geometries based on a preliminary load case.

2 MATERIALS AND EXPERIMENTAL METHODS

2.1 Mix design and materials

Three mortar mixtures were prepared with a constant water-to-binder ratio of 0.30. The reference mixture (REF) served as the control, while the Shell Reinforced Concrete (SRC) incorporated 30% crushed seashells (by volume) as a partial replacement for natural fine aggregate. In the third formulation, the Shell Glass Fiber Reinforced Concrete (SGFRC), seashell substitution was combined with the addition of glass fibers to provide dispersed reinforcement.

All mixtures contained a superplasticiser to ensure workability at the selected water-to-binder ratio (EN 934-2:2009). Silica fume was also incorporated as a pozzolanic addition to refine the microstructure and improve strength and durability (ACI 211.1-91). The detailed proportions of each component with the specific densities of the materials are presented in Table 1.

The seashells used as recycled aggregates originated from commercial mollusc residues. The material consisted of irregular, angular particles with a predominant size range of 2–5 mm (see Figure 1).

Component	REF	SRC	SGFRC	Density (kg/m^3)
Portland cement	1121.30	1197.30	1278.70	3180.00
Silica fume	33.70	36.00	33.10	2400.00
Water	346.40	367.00	430.00	1000.00
Sand	2084.30	1558.00	1663.90	2650.00
Crushed shells	—	597.40	638.00	2400.00
Glass fibers	—	—	42.60	2500.00
Superplasticizer	11.30	12.00	12.80	1000.00

Table 1: Mix compositions (kg/m^3) and material densities.

(a) Marine shells residue (b) Crushed shells as aggregate

Figure 1: Marine shells used as recycled aggregate.

The general properties of the hardened mortars were determined after 28 days of water curing. Specimens were prepared according to the requirements of each test: air permeability, capillary absorption and mechanical strength.

2.2 Air permeability test

The air-permeability of each mixture was measured with the PermeaTORR AC+ device, which applies a controlled vacuum through a double-chamber cell. The inner chamber induces airflow into the specimen, while the outer chamber seals the edges, allowing the flow to be considered essentially vertical. The measured parameter was the air permeability coefficient (k_T, in m^2), which quantifies airflow through the cementitious matrix under a pressure gradient. It is derived from the Darcy–Hagen–Poiseuille law for laminar flow, assuming unidirectional flow and a linear pressure gradient, and is expressed as:

$$k_T = \frac{Q\,\mu\,L}{A\,\Delta P}$$

where Q is the airflow rate, μ is the air viscosity, L is the equivalent penetration depth, A is the effective test area, and ΔP is the applied pressure difference. A detailed derivation of this expression and the underlying assumptions can be found in Torrent (2012).

For each mixture, one cube of $150 \times 150 \times 150$mm^3 was tested. Four lateral faces were measured on each specimen, with a 30-minute interval between consecutive determinations. Figure 2 shows the evolution of the air permeability coefficient (k_T). Reported values correspond to the daily average of all measurements.

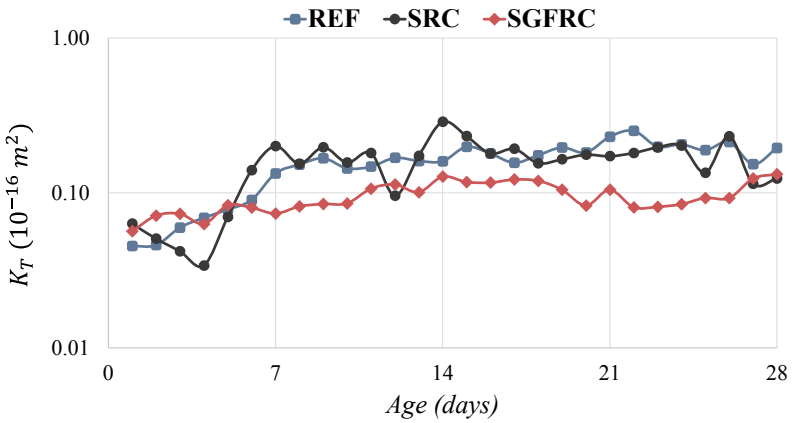

Figure 2: Daily kT measurement.

The three mixtures showed comparable air permeability, with no significant differences in the general trend. SRC showed greater fluctuations, likely related to the heterogeneity of the recycled aggregate, whereas SGFRC provided the most stable response. The 28-day k_T values and the deviations between specimen faces are summarized in Table 2.

	REF	**SRC**	**SGFRC**
k_T mean (10^{-16} m^2)	0.195	0.124	0.132
Standard deviation (between faces)	0.025	0.016	0.001

Table 2: Average air-permeability coefficient (k_T) at 28 days.

At 28 days, the mixtures with partial seashell substitution (SRC) and with glass fiber reinforcement (SGFRC) showed slightly lower permeability than the reference mixture, suggesting satisfactory potential for durability performance.

2.3 Capillary water absorption test

Capillary water absorption was determined according to EN 1015-18:2003. Specimens were oven-dried at (60 ± 5)°C until constant mass was reached, and then placed with one face in contact with a 5–10 mm water layer maintained constant throughout the test. The lateral faces were sealed with plastic film to prevent evaporation losses. The mass of the specimens was recorded at regular intervals up to 24 h. The capillary absorption coefficient (CC) was calculated as:

$$CC = \frac{M_{wet} - M_{dry}}{A \cdot \sqrt{t}}$$

where M_{wet} is the specimen mass at time t (kg), M_{dry} is the initial dry mass (kg), A is the area of the cross-section in contact with water (m^2), and t is the elapsed time (min).

Figure 3 shows the mass gain ($M_{wet} - M_{dry}$) as a function of the square root of time for the three mixtures. For each mixture, nine measurements were taken up to 24 hours, with the average CC value considered as representative.

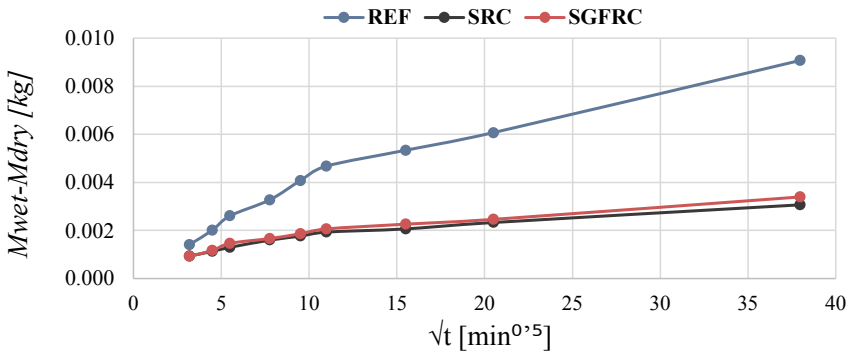

Figure 3: Capillary water absorption curves.

The REF mixture exhibited the highest absorption rate, while SRC and SGFRC showed significantly lower water absorption throughout the test period. The mean CC values at 24 hours are summarized in Table 3.

Mix	REF	SRC	SGFRC
CC [kg/(m^2 · min$^{0.5}$)]	0.149	0.051	0.056

Table 3: Capillary absorption coefficient (CC) at 24 hours.

2.4 Mechanical tests

Mechanical tests were performed according to EN 196-1:2016 on prisms measuring $160 \times 40 \times 40$ mm. The halves obtained from each flexural test were subsequently used to determine compressive strength. Table 4 summarizes the results.

Mix	Flexural strength	Compressive strength
REF	6.11	40.28
SRC	6.98	30.20
SGFRC	7.76	40.29

Table 4: Average mechanical test results (MPa)

The REF and SGFRC mixtures reached mean compressive strengths of about 40 MPa, whereas SRC showed a lower value, close to 30 MPa. In contrast, the flexural strength values were comparable across the three mixtures, indicating that the incorporation of seashells did not compromise bending performance.

3 UNIT FABRICATION AND ECOLOGICAL DEPLOYMENT

3.1 Unit design and casting

The rock-shaped units were designed to reproduce the natural inclination (20°) of the substrates where *Ericaria amentacea* settles in the intertidal zone. Each piece incorporated four holes for mechanical fixing to concrete walls (Figure 4). Six units were cast per mixture, and an additional twelve mortar discs were prepared for laboratory cultivation tests, following design criteria adopted in previous studies, Cimini (2025).

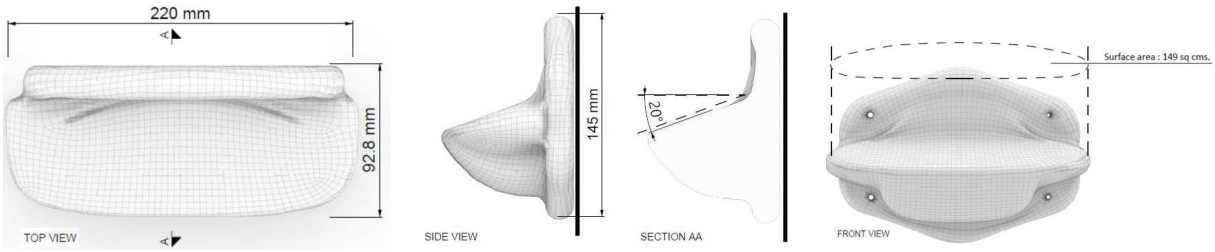

(a) Top view (b) Side view (c) Front view

Figure 4: Geometrical design of the artificial rock units (Cimini, 2025)

The units were cured for 14 days in water under standard laboratory conditions and were subsequently stored in filtered seawater until their use in cultivation.

3.2 *Ex situ* cultivation

After curing, fertile apices of *Ericaria amentacea* were placed on the surface of the units to induce gamete release and embryo attachment under controlled conditions, following protocols established in previous Mediterranean restoration studies (Falace et al., 2018) The *ex situ* cultivation started in June 2025 (see Figure 5)

(a) Discs with fertile apices (b) Units with fertile apices

Figure 5: *Ex situ* cultivation setup of *Ericaria amentacea*.

3.3 Field deployment

At the end of July 2025, half of the units were installed at Santa Margherita Ligure. This site corresponds to the intertidal zone of an artificial breakwater built after the October 2018 Vaia storm, which caused the local disappearance of *Ericaria amentacea* populations (see Figure 6)

Figure 6: Field deployment of the artificial rock units.

Evaluation in laboratory and field settings will enable long-term verification of the units' per-

formance in supporting the growth of *Ericaria amentacea* and resisting marine environmental stresses.

4 NUMERICAL IMPLEMENTATION

4.1 Method

The geometry of the units was originally defined according to biological criteria, in particular the surface inclination characteristic of natural substrates where *Ericaria amentacea* establishes in the intertidal zone. However, this configuration does not account for mechanical considerations, which may compromise the resistance of the units under marine fatigue loading.

To preserve the biologically required inclination, while improving structural performance, a first approach is proposed based on shape and topology optimization. It aims at reducing *compliance* within a linear elastic regime.

The methodological framework proposed by Allaire et al. (2021) is adopted in this study, combining Hadamard shape derivatives for PDE-constrained functionals, adjoint-state formulation, construction of descent directions via Hilbertian gradient methods (extension and regularization), and an Eulerian representation of domains with the *level set* method on a fixed mesh (with *ersatz* material) and Hamilton–Jacobi evolution.

4.2 Mathematical and computational framework

The algorithm was implemented in `Gridap.jl` using the open-source package GridapTopOpt (Wegert et al., 2025), which provides scalable infrastructure for level-set-based topology optimization.

The analysis was conducted in 2D under a plane-stress assumption, using a fixed Cartesian domain representative of the characteristic cross-section of the experimental units.

$$D = (10) \times (15) \ \text{(cm)},$$

The level set function $\phi : D \to \mathbb{R}$ encodes the geometry as $\Omega = \{\phi < 0\}$ (solid) and $D \setminus \Omega$ (void), with ϕ reinitialized periodically to a signed distance for numerical robustness. To avoid remeshing, the ersatz material approach was adopted, interpolating stiffness through a smoothed characteristic function χ_η:

$$A^\varepsilon(x) = \big(\varepsilon + (1-\varepsilon)\chi_\eta(x)\big)A, \qquad 0 < \varepsilon \ll 1, \tag{1}$$

where A is the Hooke tensor and ε a small penalization factor.

The elastic state u satisfies the weak form of equilibrium

$$\int_D A^\varepsilon e(u) : e(v)\, dx = \int_D b \cdot v\, dx + \int_{\Gamma_N} t \cdot v\, ds \qquad \forall v, \tag{2}$$

with $e(u) = \frac{1}{2}(\nabla u + \nabla u^\top)$.

The objective is to minimize the compliance:

$$J(\Omega) = \int_D A^\varepsilon e(u) : e(u)\, dx, \tag{3}$$

subject to a volume constraint handled with an augmented Lagrangian with iterative update of the multiplier λ.

$$\mathcal{L}_\rho = J + \lambda\, C + \tfrac{\rho}{2} C^2, \qquad C(\Omega) = |\Omega| - V_0, \tag{4}$$

In the present case, the target volume fraction was fixed at 0.5, ensuring that the optimized design preserves 50% of the initial domain material.

Shape sensitivities are derived from Céa's Lagrangian framework Allaire et al. (2021), leading to a Hadamard-type boundary expression involving the primal solution u and the adjoint p. In practice, this boundary term is transferred to a volumetric form using the regularized delta of the level set. The descent direction is obtained by solving a Riesz problem (Hilbertian gradient smoothing), which yields the normal velocity v driving the Hamilton–Jacobi evolution:

$$\frac{\partial \phi}{\partial t} + v \, \|\nabla \phi\| = 0. \tag{5}$$

Boundary conditions were imposed as follows: a Dirichlet condition of full clamping on the left edge,

$$u = 0 \quad \text{on } \Gamma_D = \{x = 0\},$$

and a Neumann condition on the central 20% of the right edge, consisting of a uniform surface load applied vertically downward,

$$t = (0, -1) \quad \text{on } \Gamma_N \subset \{x = 10\}.$$

This setup represents a vertical load case.

To preserve the biologically motivated surface inclination of 20°, a hard geometric mask was imposed after each Hamilton–Jacobi step:

$$\pi_{20}(x, y) = y - 15 + \tan(20^\circ)\, x, \qquad \phi \leftarrow \max\left(\phi,\ \pi_{20}\right). \tag{6}$$

with the solid defined as $\{\phi < 0\}$, this projection enforces a void wedge above the inclined boundary throughout the optimization.

Each iteration thus consists of: (i) solving the state and adjoint problems with $A^\varepsilon(\phi)$, (ii) evaluating compliance and constraint contributions, (iii) computing the smoothed descent velocity via the Riesz problem, (iv) updating the level set through the Hamilton–Jacobi equation, and (v) applying the 20° geometric mask.

4.3 Numerical results and discussion

The results for the imposed boundary conditions at different optimization iterations are shown in Figure 7.

Under a unit vertical load applied to a central subsegment of the *right* boundary, with the *left* boundary clamped, the optimized layout transferred loads through diagonal compression fields emanating from the loaded zone toward the support, balanced by a tensile path along the opposite side. Consequently, the algorithm removed material from regions that contributed little to stiffness and concentrated it along shorter, strut-like load paths, while preserving the no-material wedge enforced by the 20° mask.

These results should be regarded as a highly simplified model, formulated in 2D under plane-stress assumptions, which does not capture the inherently three-dimensional nature of the real problem.

The topology obtained is specific to the applied load case and cannot be generalized without incorporating more realistic scenarios.

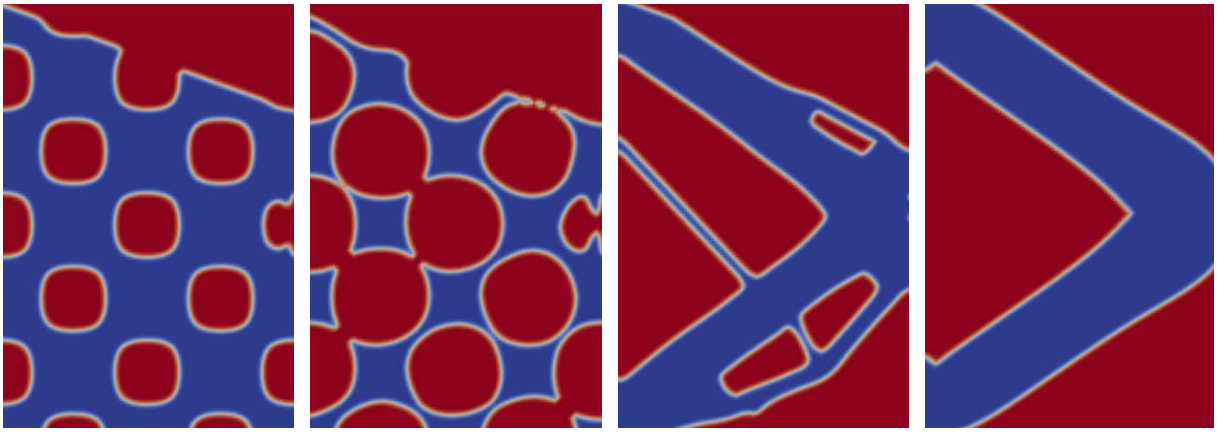

(a) Iteration 10 (b) Iteration 40 (c) Iteration 120 (d) Iteration 170

Figure 7: Shape evolution of the optimized domain at different iterations.

5 CONCLUSIONS

This study demonstrates that incorporating crushed seashells into cementitious mixtures is a viable strategy for developing substrates intended for the restoration of *Ericaria amentacea*. The tested formulations maintained flexural strength at levels comparable to the reference mixture while reducing air permeability and capillary absorption, two properties that are critical for durability in marine environments exposed to wetting–drying cycles. However, a reduction in compressive strength was observed compared to the reference material. The addition of glass fibers helped preserve compressive strength and improve toughness. These findings highlight the potential of the proposed approach for the design of more sustainable restoration materials.

In parallel, an initial computational study was carried out using shape and topology optimization based on a *level set* approach on a fixed Cartesian mesh. The algorithm incorporated the biologically motivated inclination constraint and, under a preliminary static load case, produced mechanically informed geometries with reduced *compliance*. The optimized designs revealed diagonal strut-and-tie load paths consistent with the applied boundary conditions. However, this work presents important limitations: the analyses were restricted to a 2D linear elastic model, under static loading and without considering the real wave spectrum. Future work will address these aspects simultaneously with the development of low-clinker “green concrete” binders, providing the basis for the next research stages.

ACKNOWLEDGMENTS

This work was partially financed by the EU’s Horizon 2020 research and innovation programme under the Marie Skłodowska-Curie Staff Exchange action (Grant Agreement No. 101086440 – Project acronym: BEST, Bio-based Energy-efficient materials and Structures for Tomorrow), https://cordis.europa.eu/project/id/101086440. It is a contribution to the project “National Biodiversity Future Center - NBFC”, funded under the National Recovery and Resilience Plan (NRRP), Mission 4 Component 2 Investment 1.4 - Call for tender No.3138 of 16 December 2021, rectified by Decree n.3175 of 18 December 2021 of Italian Ministry of University and Research funded by the EU – NextGenerationEU; Award Number: Project code CN_00000033, Concession Decree No. 1034 of 17 June 2022 adopted by the Italian Ministry of University and Research, CUP D33C22000960007. It is also part of the project REEForest-LIFE (101074309 LIFE21-NAT-IT-REEForest) funded by LIFE financial instrument of the EU Community.

REFERENCES

Allaire G., Dapogny C., and Jouve F. Shape and topology optimization. In A. Bonito and R.H. Nochetto, editors, *Geometric Partial Differential Equations – Part II*, volume 22 of *Handbook of Numerical Analysis*. Elsevier, 2021. http://doi.org/10.1016/bs.hna.2020.10.004. HAL: hal-02496063.

Cavaleri L., Barbariol F., Bertotti L., Besio G., et al. The 29 october 2018 storm in northern italy: Its multiple actions in the ligurian sea. *Progress in Oceanography*, 201:102715, 2022. http://doi.org/10.1016/j.pocean.2021.102715.

Chemello S., Signa G., Mazzola A., Ribeiro Pereira T., Sousa Pinto I., and Vizzini S. Limited stress response to transplantation in the mediterranean macroalga ericaria amentacea, a key species for marine forest restoration. *International Journal of Environmental Research and Public Health*, 19(19):12253, 2022. http://doi.org/10.3390/ijerph191912253.

Cimini J. *Rest-Art Project: Restoration of Marine Forests on Artificial Reefs*. Ph.D. thesis, University of Genoa, 2025. http://doi.org/https://hdl.handle.net/11567/1252516.

Falace A., Kaleb S., De La Fuente G., Asnaghi V., and Chiantore M. Ex situ cultivation protocol for *Cystoseira amentacea* var. *stricta* (fucales, phaeophyceae) from a restoration perspective. *PLOS ONE*, 13(2):e0193011, 2018. http://doi.org/10.1371/journal.pone.0193011.

Filbee-Dexter K. and Wernberg T. Rise of turfs: A new battlefront for globally declining kelp forests. *BioScience*, 68(2):64–76, 2018. http://doi.org/10.1093/biosci/bix147.

Lata L.F.L.B. and Rocha C.A.A. Processamento e caracterização de agregado miúdo de casca de mexilhão. In *Anais do 6º Encontro Nacional sobre Aproveitamento de Resíduos na Construção Civil (ENARC)*, pages 1–12. ENARC / ANTAC, Belém, Brasil, 2019.

Leite L.P., de Andrade F.K.G., Estolano A.M.L., de Almeida Filho R.R., da Cruz F.M., and de Lima V.M.E. Desenvolvimento e caracterização de concreto sustentável com resíduos de conchas marinhas. *Ambiente Construído*, 24:e131502, 2024. http://doi.org/10.1590/s1678-86212024000100723.

Torrent R. Non-destructive air-permeability measurement: from gas-flow modelling to improved testing. In *Proc. 2nd Int. Conf. on Microstructural-related Durability of Cementitious Composites*. Amsterdam, The Netherlands, 2012.

Wegert Z.J., Manyer J., Mallon C.N., et al. Gridaptopopt.jl: a scalable julia toolbox for level set-based topology optimisation. *Structural and Multidisciplinary Optimization*, 68(22), 2025. http://doi.org/10.1007/s00158-024-03927-3.